



HAL
open science

Analysis of a variable density turbulent jet submitted to a pulsed coflow

Marc Saudreau, Yannick Bury, Jacques Borée, Olivier Simonin, Georges Charnay

► **To cite this version:**

Marc Saudreau, Yannick Bury, Jacques Borée, Olivier Simonin, Georges Charnay. Analysis of a variable density turbulent jet submitted to a pulsed coflow. International Conference on Variable Density Turbulent Flows, Jun 2000, Banyuls-sur-mer, France. pp.0. hal-04104644

HAL Id: hal-04104644

<https://hal.science/hal-04104644>

Submitted on 24 May 2023

HAL is a multi-disciplinary open access archive for the deposit and dissemination of scientific research documents, whether they are published or not. The documents may come from teaching and research institutions in France or abroad, or from public or private research centers.

L'archive ouverte pluridisciplinaire **HAL**, est destinée au dépôt et à la diffusion de documents scientifiques de niveau recherche, publiés ou non, émanant des établissements d'enseignement et de recherche français ou étrangers, des laboratoires publics ou privés.



Open Archive Toulouse Archive Ouverte (OATAO)

OATAO is an open access repository that collects the work of Toulouse researchers and makes it freely available over the web where possible.

This is an author-deposited version published in: <http://oatao.univ-toulouse.fr/>
Eprints ID: 6509

To cite this document: Saudreau, Marc and Bury, Yannick and Boree, Jacques and Simonin, Olivier and Charnay, Georges *Analysis of a variable density turbulent jet submitted to a pulsed coflow*. (2000) In: International Conference on Variable Density Turbulent Flows, 22-23 Jun 2000, Banyuls-sur-mer, France.

Any correspondence concerning this service should be sent to the repository administrator: staff-oatao@inp-toulouse.fr

Analysis of a variable density turbulent jet submitted to a pulsed coflow

Saudreau, M.¹, Bury, Y. J., Borée², O., Simonin, and G., Charnay
IMFT, Ave. du Prof. Soula, 31 400 Toulouse - France

Abstract

An experimental and numerical work dedicated to the study of a variable density jet submitted to a time-varying coflow with high acceleration / deceleration levels is presented in this paper. To deal with this complex unsteady flow a simple model taking into account advective effects has been developed. It permits to bring to the fore that advective effects are responsible for a front creation during acceleration phase. This front will interact with the downstream jet structure and modify turbulence and mixing properties. As this study is linked with industrial application we simulated the entire flow by a standard $k - \varepsilon$ model. Comparisons with LDV measurements are presented and discussed.

1. INTRODUCTION.

Turbulent mixing of a jet exhausting in a different density coflow is met in numerous industrial situations. The present work is directly linked with development of natural gas vehicles (NGV) which have a high potential to reduce urban air pollution. In such spark ignition engine, the injected gaseous fuel in the intake ports ($\frac{\rho_{fuel}}{\rho_{air}} = 0.55$) is submitted to a pulsed air flow where acceleration can reach $3000g$ values (g is the gravity acceleration field). Knowledge

¹saudreau@imft.fr

²borée@imft.fr

of the mixing processes in those particular unsteady conditions is useful to optimize combustion (Fulachier,1989). Previous study concerning light jet in a pulsed crossflow (Bury,1997;Raud, 1999) has shown the complex 3D influence of this unsteadiness on the global behavior of the jet. In the present work and owing to the complexity of measurements in real engines, a model experimental setup, considering a variable density turbulent jet exhausting in a strongly pulsed coflowing duct flow, has been developed to isolate and analyse the main physical mechanisms governing such unsteady flows.

2. EXPERIMENTAL AND NUMERICAL SETUP.

2.1. Experimental setup.

The experimental setup (Bury,2000) is sketched in figure 1. It consists of a $D = 4mm$ diameter cylindrical tube jet confined in a $60 \times 60mm^2$ transparent square duct. The use of a sonic nozzle ensures a time-constant mass flux jet. Nozzle location is optimized in order to obtain a fully developed turbulent pipe flow with a $U_0 = 60m/s$ axial velocity at the jet exit. The total length of the duct generating the coflow is $2.40m$. The channel flow is generated by a vacuum pump and pulsed thanks to a motorized butterfly valve at a $f = 75Hz$ frequency. Pulsation is tuned with the channel acoustics and corresponds to a half-wave mode (Charnay, 1976). Duct entrance is a pressure node. As a result, for about thirty jet diameters downstream the duct inlet, including test section, coflow velocity U_∞ is quasi-uniform and varies from 5 to $30m/s$ with time (see fig.2). The jet therefore develops in a spatially uniform, time varying coflow. Resulting values of acceleration/deceleration \dot{U}_∞ rise up from $+400g$ to $-700g$.

To bring to the fore main effects governing such a flow, light, homogeneous and heavy jets are studied. Density variations are obtained considering an air channel flow and successively air, CO_2 ($\frac{\rho_{CO_2}}{\rho_{air}} = 1.6$) and an air-helium mixture ($\frac{\rho_{mix}}{\rho_{air}} = 0.55$) jet flow. The corresponding Reynolds numbers, based on outlet jet diameter, vary from 9,000 to 30,000, depending on the initial density. The study focuses from 0 to 25 diameters downstream the jet outlet. Particular care has been taken considering experimental boundary conditions, in view of numerical simulation comparison. To do so, a convergent type collector and a grid, placed at the duct entrance (fig.1), just upstream the studying zone, generate uniform coflow velocity profile and isotropic homogeneous turbulence, and minimize the influence of the jet tube's wake.

In order to observe the jet as it interacts with the main flow and to quantify

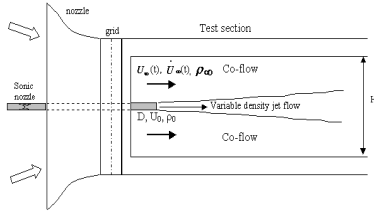


Figure 1: Presentation of the test section

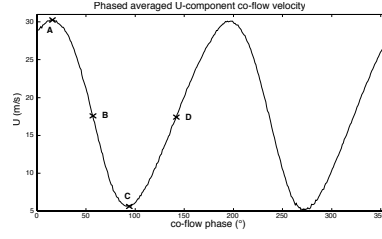


Figure 2: Coflow velocity U_∞ time evolution. (A : $U_\infty(t) = 30$ m/s, B: $U_\infty(t) = 17.5$ m/s deceleration, C: $U_\infty(t) = 5$ m/s and D: $U_\infty(t) = 17.5$ m/s acceleration)

those effects, two-component laser Doppler velocimetry (Dantec BSA) and optical concentration measurements based on Mie scattering are used and adapted to unsteady conditions. Axial velocity measurements from 0 to 25 jet diameters and radial profiles respectively at 0, 5, 10, 15, 20 diameters downstream jet outlet were achieved. For each injected fluid (air, CO₂ and air-helium mixture jets), measurements were performed under the four following coflow conditions: unsteady coflow, steady coflow at respectively $U_\infty = 5$ m/s, $U_\infty = 17.5$ m/s, $U_\infty = 30$ m/s (corresponding to unsteady phases A, B, C, D in fig 2).

2.2. Numerical study.

RANS code Estet-Astrid (Laurence & al, 1994) has been used to perform and test turbulence closure scheme for this flow. Continuity, momentum and scalar transport equations are resolved in a Favre averaging formulation. Turbulence closure used is standard $k - \varepsilon$ model adapted to axisymmetric jet, and $R_{ij} - \varepsilon$ standard model. For scalar quantities coupled with dynamic field, turbulence closure is performed using a constant Schmidt turbulence number set to 0.7 in our case. Boundary conditions are set using experimental phased averaged quantities for both coflow and jet inlet. To achieve comparison with experiment, we simulate the entire test section (fig.1), starting from grid position to 30 diameters downstream. For computational facilities we consider a cylindrical duct which radius is set to obtain the same experimental coflow mass flow rate. Thus a 2D axisymmetric computation can be performed.

As experimental duct flow is driven by pressure gradient variation, pulsation is simulated in the same way. We impose a variable outlet pressure $P_1(t)$ and a constant coflow inlet charge. Thus at each time step, duct velocity $U_\infty(t)$

fits to impose pressure gradient. Taking into account linear frictional losses, we reproduce closely experimental velocity variation show in figure.2.

In practical, the first step of simulation consists of calculating stationary axisymmetric jet with coflow velocity equal to $30m.s^{-1}$. In a second step starting from this stationary jet, duct velocity is pulsed during two periods. During the first period, the initial condition is evacuated and only the second one is compared with experimental results.

3. ON THE LONGITUDINAL DEVELOPMENT OF THE PERTURBATION.

3.1. Experimental results.

The axial evolution of the mean longitudinal velocity at phases A, B, C, D (fig.2) is displayed in figure 3 for the light jet. Each result is then compared with steady coflow velocity measurements in fig.4 and 5. A very large amplitude variation of the axial velocity is detected in figure 3. The axial velocity at phase C, corresponding to the end of the deceleration phase, is much lower than the velocity for a corresponding steady coflow $U_{\infty} = 5m/s$ (fig.5). On the contrary, the mean axial velocity at the end of the acceleration phase (A) is higher than the velocity for a corresponding steady coflow $U_{\infty} = 30m/s$. At phases B and D, the instantaneous coflow velocity seen by the jet is the same ($U_{\infty} = 17.5m/s$). The acceleration (respectively deceleration) value are however maximum. figure 4 shows that the longitudinal evolutions of axial velocity for phases B and D lie on both sides of the steady coflow case $U_{\infty} = 17.5m/s$. Similar behaviour is observed for homogeneous and heavy jets.

3.2. Physical analysis - derivation of an hyperbolic model

Momentum equation governing our flow can be derived from Navier Stokes equations using classical hypothesis for quasi-parallel and turbulent flows. Since the flow is axisymmetric we will denote by $(U(x, r, t), V(x, r, t), W(x, r, t))$ mean velocity component in cylindrical coordinate system (x, r, θ) for axial, radial and azimuthal direction. In external region flow is governed by pressure gradient and since confinement is negligible (Bury, 2000), governing equation reads (Borée, 2000) :

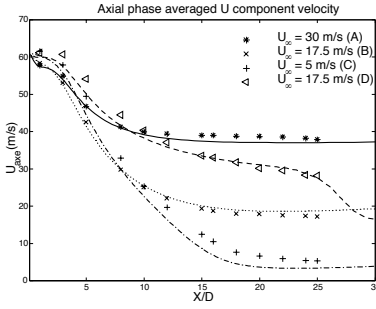


Figure 3: Light jet case comparison of U_{cl} evolution between measurements (symbol) and $k-\epsilon$ simulation (lines)

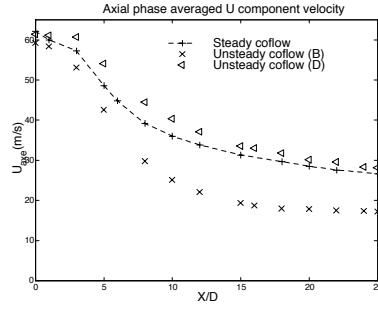


Figure 4: Light jet case comparison of U_{cl} evolution between steady and unsteady coflow for $U_{\infty} = 17.5$ m/s

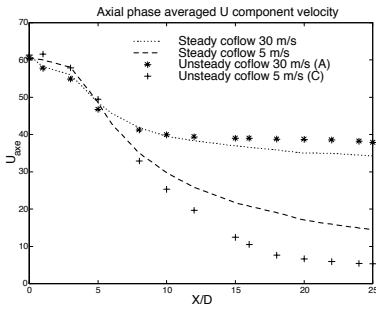


Figure 5: Light jet case comparison of U_{cl} evolution between steady and unsteady coflow for $U_{\infty} = 5$ m/s and $U_{\infty} = 30$ m/s

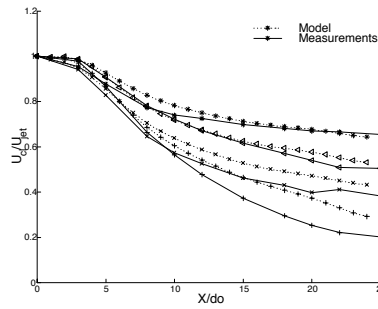


Figure 6: Centerline velocity decay comparison between measurements and model with initial condition of 17.5 m/s

$$\underbrace{\frac{\partial}{\partial t}(U - U_{\infty})}_{t1} + \underbrace{U \frac{\partial}{\partial x}(U - U_{\infty}) + V \frac{\partial}{\partial r}(U - U_{\infty})}_{t2} = \frac{1}{\rho} \Sigma_T + \underbrace{\frac{(\rho - \rho_{\infty})}{\rho} \cdot \frac{\partial U_{\infty}}{\partial t}}_{t4} \quad (1)$$

Time variation of mean excess momentum along the fluid particle trajectory is due to turbulent diffusion ($t3$) and to unsteady buoyancy term ($t4$). In the following we will consider only situations where buoyancy term is strictly zero (air jet) or small compared to other equation terms. Buoyancy contribution is detailed in (Borée, 2000).

The time variation of mean excess momentum $U(0, r, t) - U_{\infty}(t)$ is im-

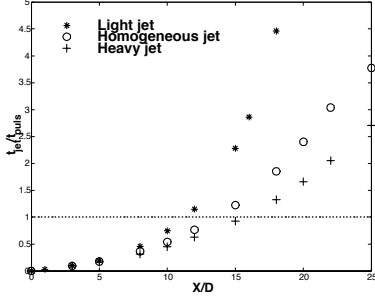


Figure 7: Time scale comparison at phase C ($U_\infty = 5m/s$)

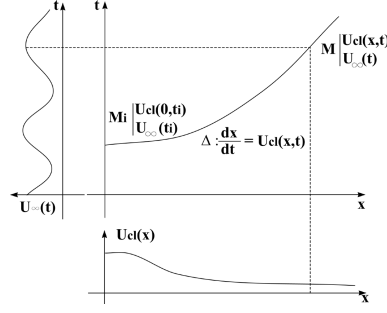


Figure 8: Characteristic method

posed at the exit of the jet. $U(0, r, t) - U_\infty(t)$ increases during deceleration phase and decreases during acceleration phase. The jet response then clearly results from a competition between these variations imposed at the time scale $t_{puls} = \max \left| \frac{\Delta U_\infty}{U_\infty} \right|$ and the mean advection and diffusion of the perturbation by the jet structure.

In steady coflowing jets, mean advection and turbulent diffusion are in equilibrium and have therefore time scales of the same order of magnitude : $t_{jet} \approx \frac{X}{U_{cl}}$ where U_{cl} is the mean centerline velocity and X the downstream distance from jet exit. Note that t_{jet} increases strongly versus axial distance ($t_{jet} \approx (\frac{X}{D})^2$ in a free steady jet). t_{jet} is compared to t_{puls} at phase C in figure 7 where light, homogeneous and heavy jets are considered. One sees clearly that while the early development of the jet is quasi-steady ($t_{jet} \ll t_{puls}$), both time scale are of the same order of magnitude for all jet at about $\frac{X}{D} = 15$. The state of this turbulent flow is therefore intermediate between quasi-steady and rapidly distorted flows.

A simple physical model can be built to describe the spatio-temporal evolution of the centerline mean velocity $U_{cl}(x, t)$ for homogeneous jet flows. If one assumes that the relative variation of mean excess momentum obtained at a given location x as a fluid particle travels over distance δx is the same in unsteady and steady situation. Considering fluid particles, their trajectories in (x, t) diagram correspond to characteristic curves (Δ) of equation : $\frac{dx}{dt} = U_{cl}(x, t)$. Along these curves, if we note by $(.)^0$ stationary quantities, the hypothesis made above implies that:

$$\frac{1}{U_{cl}(x, t) - U_\infty(t)} \frac{d(U_{cl}(x, t) - U_\infty(t))}{dx} = \frac{1}{U_{cl}^0(x) - U_\infty^0} \frac{d(U_{cl}^0(x) - U_\infty^0)}{dx} \quad (2)$$

This expression can be integrated and it comes that along line (Δ) expres-

sion $\alpha = \frac{U_{cl}(x,t) - U_{\infty}(t)}{U_{cl}^0(x) - U_{\infty}^0}$ is conserved. A similar model has been used successfully in unsteady free jets (Borée,1996) and is able to reproduce experimental observations. It is important to note that equation 2 supposes an equilibrium between turbulent diffusion and instantaneous excess momentum. In particular this statement is true in the quasi-steady initial jet region as $U_{cl}(x,t) - U_{\infty}(t) \approx x^{-1}$ and then $\frac{d(U_{cl}(x,t) - U_{\infty}(t))}{U_{cl}(x,t) - U_{\infty}(t)} \approx x^{-1} dx$ whatever the phase (Bury, 2000).

In practical solution is advanced in time along lines (Δ) by setting α as a constant (figure 8). This methodology is the same as characteristic method used for solving hyperbolic equation (Whitham,1973). Considering a fluid particle starting from jet exit ($x = 0$) at time t_i , its velocity is $U_{cl}(0, t_i)$ and the current velocity coflow $U_{\infty}(t_i)$. At time $t > t_i$ the fluid particle have been convected at local speed $U_{cl}(x,t)$ to the station $x(t) = \int_{t_i}^t U_{cl}(x(s), s) ds$. At this new location its velocity is given by:

$$U_{cl}(x,t) - U_{\infty}(t) = \underbrace{(U_{cl}(0, t_i) - U_{\infty}(t_i))}_{t1} \cdot \underbrace{\frac{U_{cl}^0(x) - U_{\infty}^0}{U_{cl}^0(0) - U_{\infty}^0}}_{t2} \quad (3)$$

Term t1 represents the initial excess momentum viewed by fluid particle at time t_i and term t2 is related to the role of turbulent diffusion according to stationary jet. Thus relation 3 expresses that mean excess momentum at (x, t) is therefore not associated to the current mean excess momentum at ejection $U_{cl}(0, t) - U_{\infty}(t)$ but to $U_{cl}(0, t_i) - U_{\infty}(t_i)$. This observation illustrates the phase lag due to convective effects in the jet structure. In particular, the dissymetry observed between acceleration and deceleration phase in figure 4 is clear. Deceleration (resp. acceleration) is associated to lower (resp. higher) initial mean excess momentum $U_{cl}(0, t_i) - U_{\infty}(t_i)$. We present in figure 6 model and measurements results for the homogeneous jet when initial condition corresponding to stationary coflowing jet with $U_{\infty}^0 = 17.5m/s$. The pulsation used for $U_{\infty}(t)$ is the experimental pulsation shown in figure 2. As a first result, the flapping of the jet centerline velocity is well reproduced. Second important point is that we mimic differences between phases B (Symbol \times) and D (Symbol \triangleleft). Thus hyperbolic model permits to explain jet structure differencies between acceleration and deceleration phases.

Following with this model, we can now consider two simple experiments. A first one we consider a stationary coflowing jet at time t_0 . At time $t > t_0$ we decrease coflow velocity (deceleration) At a given station x , as centerline velocity $U_{cl}(x,t)$ decreases in time, characteristic curves diverge and unsteady adaptation of the jet can be viewed in a (x, t) diagram as expansion waves.

On the contrary, the second experiment, starting from the same stationary jet, consists to increase coflow velocity (acceleration). Thus U_{cl} will increase and jet adaptation in (x, t) diagram will present merging characteristic curves. In a certain manner as propagation of compressive wave, a shock will eventually appear. For accelerating jets this front creation has already been mentioned and leads to a strong modification of turbulence and mixing process (Zhang, 1996).

4. EFFECT OF COFLOW ACCELERATION PHASE ON FLOW STRUCTURE - COMPARISON WITH $k - \epsilon$ MODEL

4.1 Unsteady adaptation of the jet structure.

To deal with accelerating case, we plot in figure 9 for different downstream distances from jet exit, unsteady longitudinal velocity gradient $\frac{\partial U_{cl}}{\partial x}$ adimensionalized by steady longitudinal velocity gradient for coflow velocity of $5m/s$ versus time. We note a strong peak at $\frac{x}{D} = 15$ and downstream to $\frac{x}{D} = 25$. We note also that its intensity increases with downstream distance. This high longitudinal velocity gradient $\frac{\partial U_{cl}}{\partial x}$ appears during acceleration phase (90° to 130°) and corresponds to a break in U_{cl} decaying slope. As previously discussed this phenomenon can be viewed as a consequence of the convergence of characteristic curves. Thus for $\frac{x}{D} < 10$ the longitudinal gradient does not strengthen since the jet is quasi-steady. In fact both three jets present an maximum of the local acceleration but the light jet acceleration is twice larger than the homogeneous and heavy jet acceleration. So only the light jet is presented.

Since we know maximum gradient location at any time, we are able to find its propagation law and deduce its velocity. It propagates at constant velocity V_{front} but depends on density ratio (Figure 10). For heavy jet $V_{front} \simeq 46m/s$, for homogeneous jet $V_{front} \simeq 28m/s$ and for the light jet $V_{front} \simeq 19m/s$. Similar phenomenon have been found out by Zhang & al (Zhang, 1996) for accelerating homogeneous turbulent axisymmetric jet. In case of an imposed constant acceleration of the jet exit velocity, a front is created and is propagated at constant speed. They find out that front development is mainly controlled by upstream velocity variation. In our case during acceleration phase and at a fixed downstream position near the jet nozzle $U_{cl}(x, t)$ increases in a quasi-linear fashion in time. Referring to Zhang article this could explain our constant front velocities. It should be noted that those velocities differ accord-

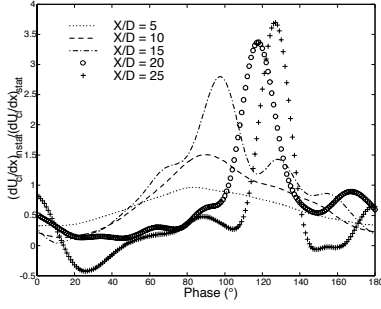


Figure 9: Temporal evolution of mean longitudinal velocity gradient for light jet at different downstream distance from jet nozzle

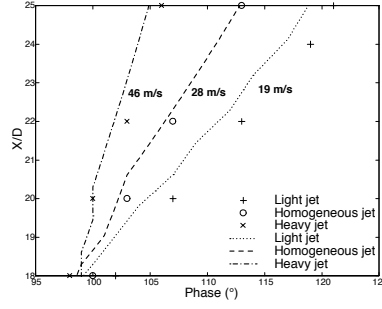


Figure 10: Downstream evolution of front during acceleration phase (from phase C to D). Symbols : measurements and lines : $k - \epsilon$ calculations

ing to jet initial density. This is directly linked with centerline velocity decay law for inhomogeneous jet. Thus a lower velocity front is then expected when initial jet density decrease.

Physically and referring to previous hyperbolic model this phenomenon is due to increase of mean velocity near jet exit in the beginning of acceleration phase i.e. merging of characteristic curves. The mean excess momentum stored in the jet structured during deceleration is evacuated rapidly downstream in starting jet type.

4.2 Effect on turbulence and mixing - Comparison with $k - \epsilon$ model.

In figure 11 longitudinal u' and radial v' rms velocity are plotted versus radial distance at location $\frac{X}{D} = 20$ for three phases during coflow acceleration. One before (90°), second during (120°) and third after (160°) front passage. As a first result the longitudinal gradient $\frac{\partial U_{cl}}{\partial x}$ dramatically increases $\langle u^2 \rangle$ component via turbulent energy production (from 90° to 120°). Secondly anisotropy is enhanced as the front propagates and decreases behind the front when energy produced on $\langle u^2 \rangle$ component is transferred to $\langle v^2 \rangle$ and $\langle w^2 \rangle$ components.

$k - \epsilon$ simulation result is shown in figure 12. Longitudinal rms velocity u' is deduced from turbulent energy k as $u' = \sqrt{\frac{2}{3}k}$. Of course since $k - \epsilon$ model is based on isotropic turbulence hypothesis, it can obviously not mimic anisotropic but turbulence production due to longitudinal gradient $\frac{\partial U_{cl}}{\partial x}$ is well simulated but its intensity is lower than measured one.

In figure 13 is plotted mean centerline density profile versus downstream

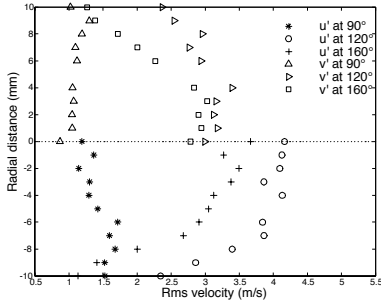


Figure 11: Turbulence production due to mean longitudinal velocity gradient at $\frac{X}{D} = 20$

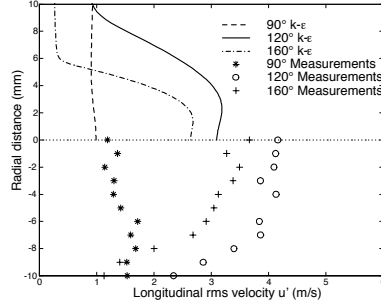


Figure 12: Experimental turbulence production (Symbols) during acceleration phase. Comparison with $k - \epsilon$ prediction (Solid lines)

distance during front propagation. As a first results mixing process is modifying since decaying slope presents a strong longitudinal density gradient located near $\frac{X}{D} = 15$. $k - \epsilon$ simulation overestimates longitudinal gradient and as a consequences mispredicted front intensity. This problem deals with model constants which are adjust for axisymmetric turbulent jet case. In our case, in flow region where the jet dominates ($t_{jet} < t_{cofl}$ i.e. near jet exit) simulation works well. Thus front velocities are correctly captured (Figure 10). On the contrary in flow region where outer pressure gradient effects are stronger ($t_{jet} > t_{cofl}$) flow behaviour is mispredicted and leads to an overestimation of front intensities (Figures 3 and 13).

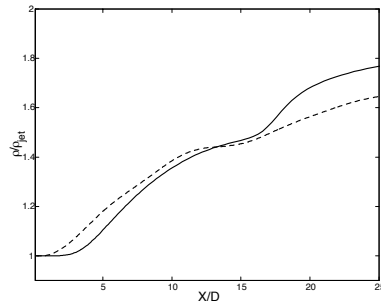


Figure 13: Density profil at phase 110° . Dashed line : measurements and solid line : $k - \epsilon$

In the view of industrial application we choose to simulate our flow using a standard $k - \epsilon$ model which is widely used for engine calculation. As a first result this model works pretty good as it mimics the time evolution of the jet and front creation (figure 3) whatever initial jet density (figure 10). Nevertheless to deal with anisotropic turbulent production and unsteady buoyancy effects, higher order models are necessary to improve situation prediction. To do so $R_{ij} - \epsilon$ and *L.E.S.* calculations are actually performed and results are still under investigation.

5. CONCLUSION.

This work based on experimental coupled with numerical study permits to bring to the fore main physical effects governing a turbulent jet submitted to a pulsed coflowing stream.

The use of a hyperbolic model derived from momentum equation for centerline mean excess velocity has shown that jet response in a non quasi-static fashion. During acceleration phase the external coflow pulsation leads to a front formation which deeply modifies jet properties. Production of turbulence is enhanced in an anisotropic way and mixing process is modified by comparison with stationary jet mixing.

Standard $k - \epsilon$ model show good agreement with measurements in the limits of its possibility. Other simulation based on $R_{ij} - \epsilon$ and Large Eddy Simulation will permit to study turbulence modification in this flow during front propagation.

In the view of industrial application, this study shows that unsteady flows can not be deduced directly from stationary ones. Unsteady flows imply memory effects, different time adaptation, phase lag effects and need inevitably to be studied. Thus simple experiments and numerical studies have to be done to isolate main unsteady physical effects governing such flows. Thus by constant comparison between experiment and simulation classical physical models used in numerical tool can be tested and improved.

References.

Borée, J., Atassi, N., Charnay, G. (1996)

Phase averaged velocity field in an axisymmetric jet subject to a sudden velocity decrease., *Experiments in Fluids*, Vol 21, pp 447-456

Bury, Y., Raud, N., Bazile, R., Borée, J., Charnay, G. (1997)

Jet fortement chauffé soumis à un écoulement instationnaire de conduite, con-

grès SFT 97 -Thermique aéronautique et spatiale,pp 408-413

Bury, Y., Saudreau, M., Borée, J.,Charnay, G. (2000)

Experimental and numerical study of a confined variable density turbulent jet submitted to a strongly pulsed coflow, congrès THMT3

Charnay G. and Matthieu J. (1976)

Periodic Flow in a Wind-Tunnel Produced by Rotating Shutters., ASME Journal of Fluids Engineering, Vol. 98, pp.1-6.

Fulachier L., Borghi R., Anselmet F., Paranthoen P. (1989)

Influence of Density Variations on the Structure of Low-Speed Turbulent Flows: a Report on Euromech 237, Journal of Fluid Mech., Vol.203, pp.577-593.

Laurence D., Simonin O. (1994)

Numerical Implementation of Second-Moment Closures and Application to Turbulent Jets, in Recent Research Advances in the Fluid Mechanics of Turbulent Jets and Plumes, P. A. Davies and M. J. Valente Neves (Editors), Kluwer Academic Publishers, pp 281-294. EDF HE 41/93/047/A

Raud N., Bury Y., Bazile R., Borée J., Charnay G. (1999)

Experimental Study of the Behaviour of Confined Variable Density Jets in a Time Varying Crossflow., ASME Journal of Fluids Engineering, Vol.121, pp.65-72.

Ricou, F. P. and D. B. Spalding (1961),

Measurements of entrainment by axisymmetrical turbulent jets, J. Fluid Mech., Vol 11, pp 21-32

Whitham,G.B. (1973)

Linear and nonlinear waves, Pure and applied mathematics.

Zhang Q. and Johari H. (1996),

Effects of acceleration on turbulent jets, Physics of Fluids, Vol 8(8), pp 2185-2195